Bimodal representation of the tropical intraseasonal oscillation

Kazuyoshi Kikuchi · Bin Wang · Yoshiyuki Kajikawa

Abstract The tropical intraseasonal oscillation (ISO) shows distinct variability centers and propagation patterns between boreal winter and summer. To accurately represent the state of the ISO at any particular time of a year, a bimodal ISO index was developed. It consists of Madden-Julian Oscillation (MJO) mode with predominant eastward propagation along the equator and Boreal Summer ISO (BSISO) mode with prominent northward propagation and large variability in off-equatorial monsoon trough regions. The spatial–temporal patterns of the MJO and BSISO modes are identified with the extended empirical orthogonal function analysis of 31 years (1979–2009) OLR data for the December–February and June–August period, respectively. The dominant mode of the ISO at any given time can be judged by the proportions of the OLR anomalies projected onto the two modes. The bimodal ISO index provides objective and quantitative measures on the annual and interannual variations of the predominant ISO modes. It is shown that from December to April the MJO mode dominates while from June to October the BSISO mode dominates. May and November are transitional months when the predominant mode changes from one to the other. It is also shown that the fractional variance reconstructed based on the bimodal index is significantly higher than the counterpart reconstructed based on the Wheeler and Hendon's index. The bimodal ISO index provides a reliable real time monitoring skill, too. The method and results provide critical information in assessing models' performance to reproduce the ISO and developing further research on predictability of the ISO and are also useful for a variety of scientific and practical purposes.

Keywords Tropical intraseasonal oscillation · MJO · Index

School of Ocean and Earth Science and Technology Contribution Number 8213 and International Pacific Research Center Contribution Number 798.

K. Kikuchi (✉)
International Pacific Research Center, School of Ocean and Earth Science and Technology, University of Hawaii, 1680 East West Road, POST Bldg. 401, Manoa Honolulu, HI 96822, USA
e-mail: kazuyosh@hawaii.edu

B. Wang
Department of Meteorology and International Pacific Research Center, School of Ocean and Earth Science and Technology, University of Hawaii, Manoa Honolulu, HI 96822, USA

Y. Kajikawa
Hydrospheric Atmospheric Research Center, Nagoya University, Nagoya, Japan

1 Introduction

Tropical intraseasonal oscillation (ISO) or referred to as the Madden-Julian oscillation (MJO) in honor of the discoverers (Madden and Julian 1971), characterized by the period of 30–90 (60) days, plays a fundamental role in regulating weather and affecting climate both in the tropics and extra tropics. A remarkable feature, which makes the ISO so influential in part, is its potential interactions with a variety of spatial and temporal scales such as diurnal cycle (Chen and Houze 1997; Ichikawa and Yasunari 2008), tropical cyclones (Maloney and Hartmann 2000a, b; Molinari and Vollaro 2000), El Niño (Kessler et al. 1995; Takayabu et al. 1999), annular modes (Miller et al. 2003), and monsoon systems of Asia (Yasunari 1979; Kajikawa and Yasunari 2005), Australia (Hendon and Liebmann 1990; McBride

et al. 1995), and North America (Higgins and Shi 2001; Lorenz and Hartmann 2006; Moon et al. 2010).

The fundamental feature of the ISO may be best illustrated in a longitude-height cross sections along the equator as in the schematic summary in their pioneering work by Madden and Julian (1972): A planetary scale convective anomaly consisting of mesoscale convective systems coupled with large-scale circulation disturbance with the gravest baroclinic structure moves eastward at about 5 ms^{-1} in the eastern hemisphere. In the western hemisphere, on the other hand, upper-level circulation disturbance rarely coupled with convection moves eastward at a speed of about 15–20 ms^{-1}. The circulation disturbance is associated with equatorial Kelvin and Rossby waves (Rui and Wang 1990; Hendon and Salby 1994). More thorough reviews can be found in some literatures (e.g., Madden and Julian 1994; Lau and Waliser 2005; Zhang 2005).

Such a simple description of the ISO which moves exclusively eastward, although is often used to describe the major feature of the ISO, may not necessarily be appropriate to best document the crucial aspect of the ISO throughout the year. There is observational evidence that the properties of the ISO such as activity centers and propagation patterns are strongly regulated by the annual cycle (Madden 1986; Salby and Hendon 1994; Webster et al. 1998; Zhang and Dong 2004). An example is given in Fig. 1, which shows annual variation of the ISO propagation with emphasis on the eastern hemisphere where convective systems associated with the ISO rather appear clearly. There are two distinct propagation tendencies: during boreal winter the organized convection associated with the ISO shows predominantly eastward propagation along the equator with little poleward propagation, whereas during boreal summer it shows prominent northward propagation over the northern Indian Ocean (and western North Pacific, not shown) (Yasunari 1979; Knutson and Weickmann 1987; Wang and Rui 1990) with weakened eastward propagation. The difference in propagation characteristic can account for the difference in the ISO activity centers (Kemball-Cook and Wang 2001; Zhang 2005). In addition, accompanied large-scale circulation shows rather symmetric about the equator during boreal winter, whereas it shows asymmetric during boreal summer. Thus, the simplest model with only zonal propagation component considered appears to be more relevant to document the ISO behavior during boreal winter, and a more complex model with meridional propagation component as well as zonal propagation component considered is more relevant to document the ISO behavior during boreal summer.

Consideration of such annual variation of the ISO is of critical importance for especially studies on interactions of the ISO with a widespread variety of spatial and temporal
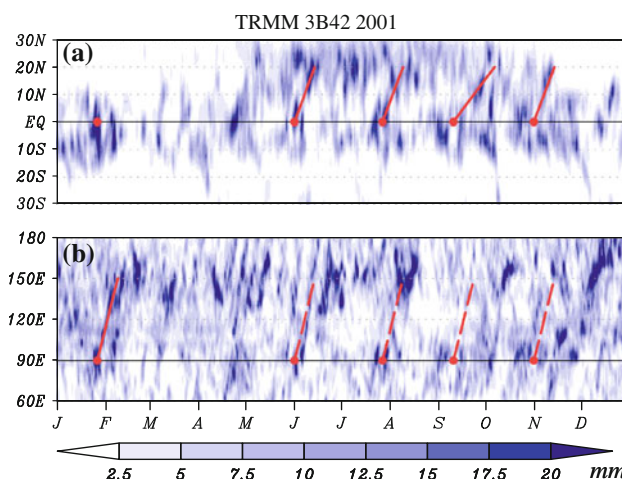
Fig. 1 Daily precipitation (tropical rainfall measuring mission product 3B42) associated with the ISO for the year 2001. **a** Latitude-time plot over the eastern Indian Ocean averaged between 80 and 100°E and (**b**) longitude-time plot along the equator between 7.5°S and 7.5°N. Each *red closed circles* indicates major convection associated with significant ISO events, determined by our analysis to be introduced in Sect. 4 (see also Fig. 4), sitting around the central Indian Ocean (90°E, 0°). *Solid* and *dashed lines* show reference phase speed corresponding to (**a**) northward propagation at approximately 1–2 ms^{-1} and (**b**) eastward propagation at approximately 6 ms^{-1}. The *solid lines* are intended to represent rather apparent convection exists

scales. A meticulous treatment of the ISO is the basis for analyses of those studies, because different structures of the ISO are expected to have different roles in weather and climate variations. In fact, for instance, Kikuchi and Wang (2010) showed that the winter type ISO and the summer type ISO have different manners in which tropical cyclogenesis are affected over the northern Indian Ocean.

The purpose of this study is to develop an ISO index which reflects such annual variation of the ISO. The index, referred to as the bimodal ISO index, relies on two distinct ISO modes, which capture the aforementioned two distinct propagation features for the two solstice seasons. With this method, the state of the ISO at any particular time can be faithfully diagnosed in terms of the two ISO modes. As a result, any ISO event can be classified into either ISO mode, which is critical information for studies of interactions of the ISO with weather and climate variations on a wide range of timescales.

A brief review of methods used to extract ISO signals is presented in Sect. 2. Section 3 describes the dataset and intraseasonal time-filter used. The bimodal ISO index is introduced in Sect. 4, which also includes some sensitivity tests and a comparison with the Wheeler and Hendon (2004) index. In Sect. 5, how the ISO can be represented with the bimodal ISO index is examined. An application of the index to real time monitoring is discussed in Sect. 6. Section 7 summarizes this study.

2 A review of methods used to extract ISO signals

Before introducing the bimodal ISO index, it is worth reviewing methods that have been used to extract ISO signals, although majority of these methods were not intended to construct an ISO index. A variety of methods have been used with various degrees of complexity. Perhaps the simplest method is to focus on an intraseasonal fluctuation of a single variable at a particular location, and document the ISO behavior based on that variability (e.g., Julian and Madden 1981; Hendon and Salby 1994), while the most meticulous and comprehensive method is a tracking method (Wang and Rui 1990; Jones et al. 2004) as it is carefully designed to depict various types of convective behaviors associated with the ISO.

Between those extremes, Eigen techniques have been widely used (Table 1). Eigen techniques provide a convenient method for the description of the spatial and temporal variability associated with the ISO in terms of empirically derived functions (spatial patterns in general). Since the ISO is characterized by organized convection coupled with large-scale circulation with the gravest baroclinic structure, such variables as convection, the upper- and lower-tropospheric circulation are relevant to isolating variations associated with the ISO. In fact, composite life cycles of the ISO based on different variables (and also different methods) produce consistent structures in the ISO behavior for any particular season (references are in Table 1).

Of particular importance is the study by Wheeler and Hendon (2004) (refer to as WH04 hereafter), pioneering work introducing all-season ISO index for real time monitoring and it has become the most popular ISO index. The

Table 1 Summary of Eigen techniques used to extract ISO signals in previous studies

Method	OLR	u_{850}	u_{200}	X_{upper}	ψ_{upper}
EOF	LC88	MH98		KW87	S99
	WH04*	WH04*	WH04*	vSX90	
EEOF	LC85, 86			KK99	
	W03, 04				
CsEOF	AS05				
SVD	ZH97*	ZH97*			
	H96*				H96*

AS05 Annamalai and Sperber (2005), *H96* Hsu (1996), *KK99* Kayano and Kousky (1999), *KW87* Knutson and Weickmann (1987), *LC85* Lau and Chan (1985), *LC86* Lau and Chan (1986), *LC88* Lau and Chan (1988), *MH98* Maloney and Hartmann (1998), *S99* Slingo et al. (1999), *vSX90* von Storch and Xu (1990), *W03* Waliser et al. (2003a, b), *W04* Waliser et al. (2004), *WH04* Wheeler and Hendon (2004), *ZH97* Zhang and Hendon (1997), *EEOF* extended EOF, *CsEOF* cyclostationary EOF, *SVD* singular value decomposition

The asterisks means multivariables are used in the corresponding eigen technique

uniqueness of their method is to use the combined variables (OLR and zonal winds at 850 and 200 hPa) meridionally averaged between 15°S and 15°N in order primarily to remove higher-frequency variability by focusing on the coherent structure of convection and large-scale circulations associated with the ISO throughout the year without use of ordinary time filters. More detailed procedure for real time monitoring is discussed in Sect. 6.

Another emphasis to be put is on the extended EOF (EEOF) analysis (Weare and Nasstrom 1982). The EEOF analysis has a unique feature that it focuses on a sequential spatial-temporal evolution by extension of the EOF analysis to a segment of consecutive times, and thereby it may be more appropriate to document a phenomenon that propagates. In other words, it can be thought to have the nature of a tracking method. With appropriate series of successive time points included, a pair of the first two EEOFs can represent a half cycle of the ISO (Lau and Chan 1985, 1986), whereas, with longer series of time points included the first EEOF alone can represent a whole cycle (Kayano and Kousky 1999) or more cycles (Waliser et al. 2003a, 2004) of the ISO.

3 Data and intraseasonal time filter

Given the data availability, our analysis is based on a 31 year dataset from 1979 to 2009 except for real-time monitoring to be discussed in Sect. 6. As mentioned in Sect. 2, referring to one or some of such variables as convection, the upper- and lower-tropospheric circulation is reasonable to isolate variations associated with the ISO. Among them the OLR data, a good proxy for organized convection in the tropics, have been widely used. Since the planetary scale convective anomaly is among the major characteristics of the ISO and of primary interest, we also used daily OLR data with 2.5° horizontal resolution (Liebmann and Smith 1996) to identify typical ISO modes and significant ISO events. Daily mean horizontal winds at 850 hPa of the Modern Era Retrospective-analysis for Research and Applications (MERRA) product (inst6_3d_ana_Np) developed by the Global Modeling and Assimilation Office (GMAO) at the NASA Goddard Space Flight Center (Bosilovich et al. 2006) were used to document large-scale circulations associated with the ISO convection. The dataset is among the state-of-the-art reanalysis, which was produced in an attempt to reduce biases stemming from observing system changes occurred over the past three decades, notably introduction of new satellites. The data with 2.5° horizontal resolution, which was created by reducing the original resolution of 2/3° × 0.5° in longitude-latitude, was used for our analysis.

To extract variations on intraseasonal timescale, Lanczos band-pass filter (Duchon 1979) with cut-off periods 25

and 90 days and 139 weights is applied to the daily OLR data and the MERRA reanalysis. This filter is referred to as the *intraseasonal time-filter* hereafter. Seventy points from either ends of the record were discarded because the full convolution cannot be performed. Because the ISO during boreal summer tends to show shorter period of near 30 days (Wang et al. 2006), the bandwidth of the band-pass filter was set somewhat wider than usual (25–90 day instead of 30–90 day). The results to be shown later are little affected no matter which bandwidth is selected.

4 Introduction to the bimodal ISO index

The main goal of this study is to develop an ISO index that faithfully represents the state of the ISO over the course of a year by taking the annual variations of the ISO behavior into account. The horizontal distribution of the ISO variance suggests that northward propagation predominates over the eastward propagation during boreal summer (see Fig. 9 in Zhang 2005). As such, in addition to the eastward propagation, capturing the northward propagation is a desirable attribute of an ideal ISO index in some seasons. With the ability to document a detailed spatial-temporal evolution, the EEOF analysis is probably most suitable for capturing such detailed propagation features. Given the observational evidence that the ISO shows contrasting behaviors between the two solstice seasons, we construct an index based on two typical ISO modes predominant for each solstice season in order that the state of the ISO are measured in terms of the properties not only during boreal winter but also during boreal winter.

4.1 The bimodal ISO index: the MJO mode and the BSISO mode

Two distinct typical ISO modes, predominant during boreal winter (referred to as the MJO mode in honor of the discoverers) and during boreal summer (referred to as the BSISO mode), are defined. To better describe the state of the ISO, we took an analogous setting for the EEOF analysis as Lau and Chan (1985, 1986); The EEOF analysis with −10 and −5 day lags was applied to the intraseasonal time-filtered OLR data in the entire tropics between 30°S and 30°N. The time lag was chosen in this way because of consideration of its application to real time monitoring. To derive the MJO (BSISO) mode the data period from December to February (June–August) was selected.

As expected from the previous studies, a pair of the first two EEOFs represents a half cycle of the ISO for both modes (Fig. 2). The MJO mode shows a predominant eastward propagation along the equator that is in accordance with the classical view of the MJO (Madden and

Julian 1972). The BSISO mode shows a prominent northward propagation over the northern Indian Ocean with weaker eastward propagation along the equator, which eventually makes an elongated convective band tilting from northwest to southeast covering a wide range from the Arabian Sea to the western Pacific. Another prominent northwestward propagation is seen over the western North Pacific. These rather complicated features of the BSISO mode are in good agreement with a recent composite study using TRMM satellite precipitation data (Wang et al. 2006). Evidently, the lifecycle of the MJO mode and the BSISO mode have distinctive characteristics.

The bimodal ISO index is based on these two ISO modes. The EEOF coefficients (principal components, PCs hereafter) of the MJO mode and the BSISO mode at any given time can be obtained by projecting the intraseasonal time-filtered OLR fields onto each mode. The strength and the phase of the MJO mode and the BSISO mode can be described by a combination of the first two PCs for each mode. This is the fundamental step for constructing the bimodal ISO index.

How to utilize the bimodal ISO index, however, might depend on analysis. In the following, we provide an example, which would be one of the most straightforward ways. For most practical applications, one may want to identify *significant ISO events* (Step 1). For that purpose, it is usual to use the normalized amplitude ($A^*_{\mathrm{mode}} = \sqrt{PC^{*2}_{1,\mathrm{mode}} + PC^{*2}_{2,\mathrm{mode}}}$), where PC^* is the normalized PC by one standard deviation during the period the EEOF analysis was performed and the subscript 'mode' represents either the MJO mode or BSISO mode. A criterion that $A^*_{\mathrm{mode}} \geq 1$ is regarded as a significant event is perhaps the most popular (e.g., Wheeler and Hendon 2004). As a result, significant ISO events can be identified in terms of the following ISO modes: (1) the MJO mode, (2) the BSISO mode, and (3) both the MJO mode and the BSISO mode.

Although, the information listed in step 1 is useful for certain analyses, in many cases it is more practical to further determine the *predominant mode*, i.e. which mode dominates the ISO event (Step 2). This can be accomplished by assuming that the predominant ISO mode at a given time accounts for a larger amount of the total variance. The reconstructed OLR anomalies by each mode at time t are given by

$$\mathbf{OLR}_{\mathrm{mode}}(t) = \mathbf{EEOF}_{1,\mathrm{mode}} \times PC_{1,\mathrm{mode}}(t) + \mathbf{EEOF}_{2,\mathrm{mode}} \times PC_{2,\mathrm{mode}}(t) \qquad (1)$$

where $\mathbf{OLR}(t)$ includes spatial patterns at −10 and −5 days as well as 0 day. With the aid of the orthogonality of the EEOF, the norm (variance) of the reconstructed pattern of each mode is given by
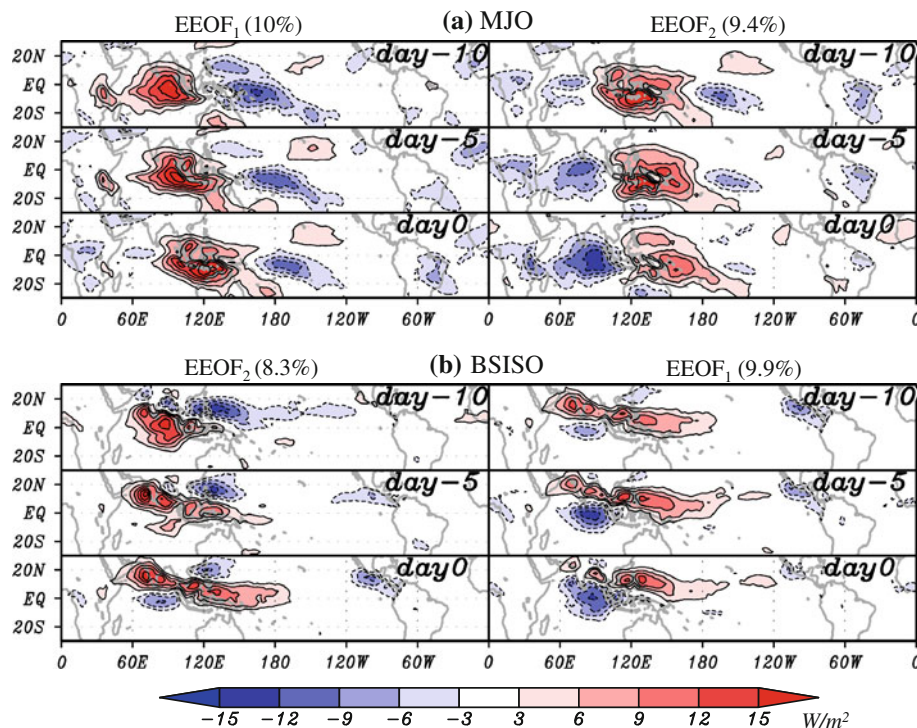
Fig. 2 Spatial-temporal pattern of OLR anomaly associated with the intraseasonal oscillation during (**a**) boreal winter (DJF, referred to as MJO mode) and (**b**) boreal summer (JJA, referred to as BSISO mode) by means of the extended EOF (EEOF) analysis. The EEOF analysis with three different time steps with 5 day time increment was applied to long-term OLR anomaly (1979–2009) with 25–90 day bandpass filter applied. The numbers in the *brackets* shows the relative contribution of each mode to total variance. OLR values are multiplied by one standard deviation of the corresponding principal components during the period each EEOF analysis was performed. Note that the EEOFs are displayed in a way that the organized convection associated with the ISO starts to appear in the Indian Ocean at day 0 in the *left panel* for convenience

$$\|\mathbf{OLR}_{\text{mode}}(t)\| = \sqrt{PC_{1,\text{mode}}^2(t) + PC_{2,\text{mode}}^2(t)} \qquad (2)$$

A comparison of (2) between the MJO mode and the BSISO mode yields the predominant mode at time t. The procedure employed in this study for identifying significant ISO events in terms of the MJO mode and the BSISO mode is summarized in Fig. 3.

To see how the procedure works, Fig. 4 shows a scatter plot of the MJO amplitude versus the BSISO amplitude represented by (2). Each of the reference solid lines provides a virtually criterion for significant ISO events in terms of either the MJO mode or the BSISO mode; the normalized amplitude, A^*, instead of the unnormalized amplitude is used to judge the state of the ISO for practical application. Note that the difference in the reference amplitude between the two modes reflects the seasonal variations in the ISO strength. Of particular importance is that there are two clusters of events that can be separated very well in the scatter plot. Most of the significant ISO events are readily assigned to either the MJO mode (region I) or the BSISO mode (region III). Even in the case when both the MJO mode and the BSISO mode have substantial
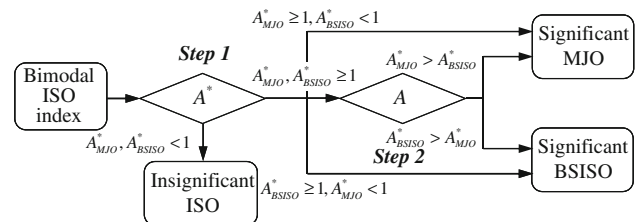

Fig. 3 Flowchart summarizes the procedure for identifying significant ISO events in terms of the MJO mode and the BSISO mode

amplitude (region II), the situation in which the two modes have almost the same amplitude rarely occurs, and hence the prevailing mode remains to be easily determined. One peculiar situation occurs when a significant BSISO event regarded as an insignificant MJO event has larger variance in terms of the MJO mode than in terms of the BSISO mode (region IV). This situation, however, is quite rare and thus how to treat it little affects the statistical analysis results. In summary, in the bimodal ISO index the state of the ISO can be expressed in terms of the MJO mode and the BSISO mode; which mode better describes at any particular time can be reasonably identified.
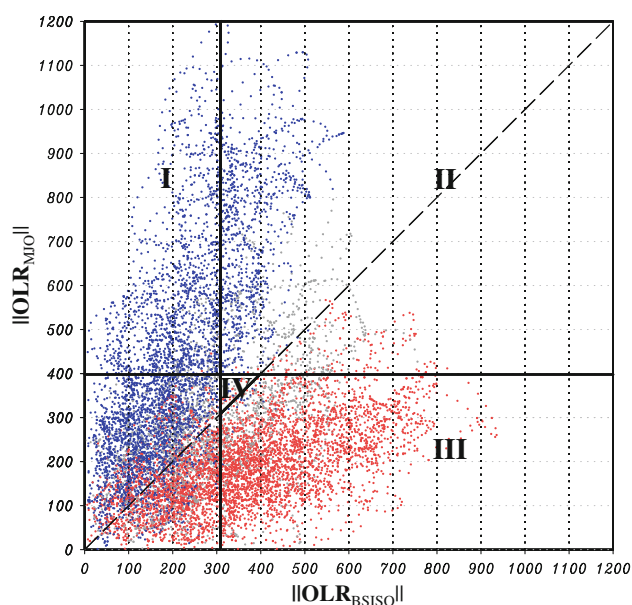
Fig. 4 Scatter plot of ISO amplitude in terms of the BSISO mode (*x* axis) and the MJO mode (*y* axis) for the period 1979–2009. *Solid lines* parallel to the *x* and *y* axes represent one standard deviation of each ISO mode ($\sqrt{PC_1^2 + PC_2^2}$) during the period each EEOF analysis was performed. *Dashed line* represents the situation when both the MJO mode and the BSISO mode have the same variance. According to the later discussion about Fig. 8, three seasons are in different colors (June–October in *red*, December–April in *blue*, otherwise in *gray*)
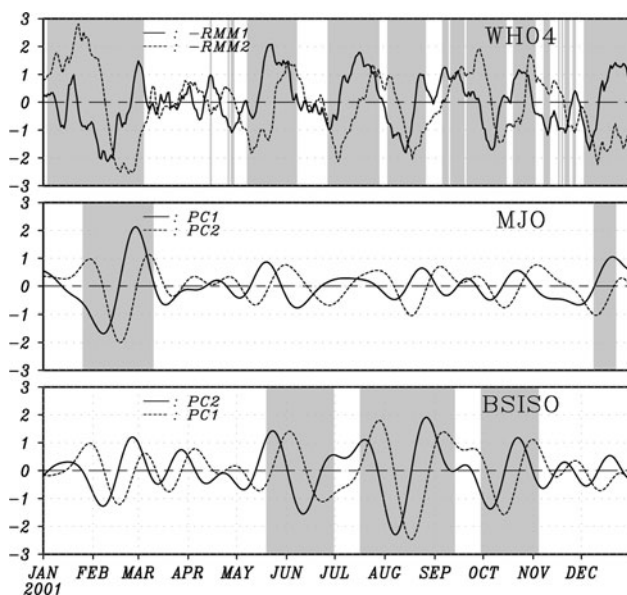
Fig. 5 A comparison of the ISO index between the WH04 (*upper*), the MJO (*middle*) and the BSISO (*lower*) for the year 2001. Note that each PC is normalized by one standard deviation of the corresponding PCs during the period each EEOF analysis was performed to obtain the EEOFs. Significant ISO events are *shaded* in the background

4.2 Comparison with Wheeler and Hendon's index

A comparison of the bimodal ISO index with WH04 index is discussed in terms of an example shown in Fig. 5. The amplitude of the WH04 index for this given year does not seem to vary significantly except in the beginning of the year when the amplitude is slightly larger than the rest of the year. The MJO mode and the BSISO mode, on the other hand, have substantial seasonal variations in amplitude. Naturally, the amplitude of the MJO (BSISO) mode is larger during boreal winter (summer). The time series of the MJO mode and the BSISO mode are smoother due to the absence of higher-frequency component than that of the WH04 counterpart.

As shown in Table 2, the correlations of the MJO mode and the BSISO mode with the WH04 index are statistically significant at the 99% level for the entire period. Of note is that the correlations of the WH04 index with both the MJO mode and the BSISO mode become larger during boreal winter. As expected, the WH04 index better represents the ISO behavior during boreal winter because of the pronounced eastward propagation and large amplitude. Significant but lower correlations during boreal summer may be a reflection that the ISO amplitude is misrepresented by the eastward propagating component alone because of the prominent northward propagation during that season. Again, the bimodal ISO index gives more detailed information on which type of the ISO mode is predominant at a particular time.

Then which ISO index better represents variations associated with the ISO? In order to answer this question, composite life cycles were constructed based on the bimodal ISO index and the WH04 index for the two solstice seasons. Figure 6 shows fractional variance explained by each composite. The patterns based on the bimodal ISO index and based on the WH04 index are in good agreement for both seasons. However, the amplitude based on the bimodal ISO index outperforms that based on the WH04 index by at least 50% in almost all regions where fractional variance has some value (≥ 0.1). This difference indicates that the ISO samples chosen based on the bimodal index are more standardized. This characteristic is another advantage of the bimodal ISO index.

5 Characteristics of the ISO behaviors in terms of the bimodal ISO index

5.1 Composite life cycle

Although, many previous studies have already documented composite life cycles of the ISO in terms of convection coupled with large-scale circulations during boreal winter

Table 2 Maximum lag correlations and the corresponding lags (*in brackets*) of the first two PCs of the MJO mode and the BSISO mode with those of the WH04 index

	MJO (PC$_1$ and PC$_2$)			BSISO (PC$_2$ and PC$_1$)		
	All	DJF	JJA	All	DJF	JJA
-RMM1	0.63 (0)	0.74 (0)	0.44 (−3)	0.60 (−1)	0.66 (−1)	0.61 (−3)
-RMM2	0.70 (0)	0.77 (−1)	0.59 (0)	0.64 (0)	0.71 (1)	0.62 (0)
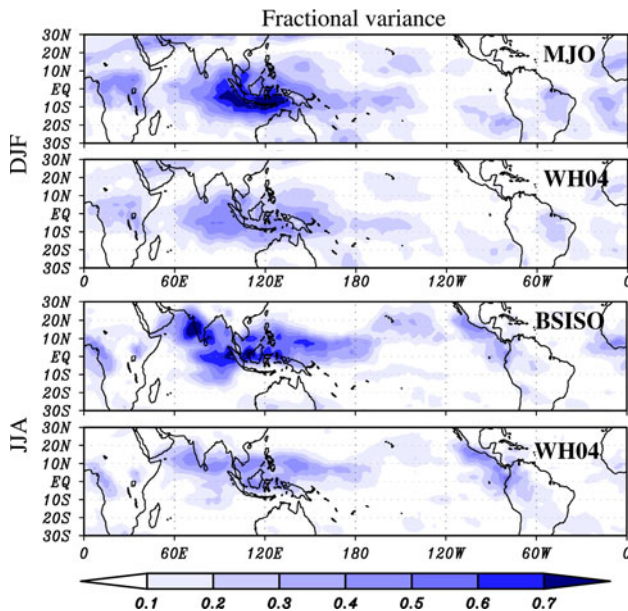
Fig. 6 Fractional variance of ISO composites in terms of OLR based on the bimodal ISO index (*upper panels*) and WH04 index (*lower panels*) during boreal winter (*left panels*) and summer (*right panels*) for the period 1979–2009. The fractional variance is defined as the ratio of the variance of the ISO composite which undergoes through its life cycle to the total variance of the intraseasonal (25–90 day) fluctuation. The composite lifecycle with WH04 index was constructed in the same manner as WH04. The lifecycle with the bimodal ISO index was constructed in a similar way, which was descried in Sect. 4.1 except that, for a fair comparison, the criterion for determining significant ISO events based on A^* was adjusted so that the total number of days (samples) used to construct the composite are the same between the two indices (1,726 for DJF and 1,579 for JJA)

(corresponding to the MJO mode) (e.g., Hendon and Salby 1994; Maloney and Hartmann 1998) and boreal summer (corresponding to the BSISO mode) (e.g., Kemball-Cook and Wang 2001; Wang et al. 2006), it is useful to show the composite life cycles based on the bimodal ISO index to confirm the results and facilitate the following discussions. Note again in this composite the ISO events are not distinguished by the seasons they occur. The use of the MERRA data updates our knowledge of large-scale circulations associated with the ISO. Composite life cycles of the MJO mode and the BSISO mode were constructed based on a phase space consisting of the first two PCs (Fig. 7). Significant MJO and BSISO events were identified in the way described in Sect. 4.1.

The composite life cycles of the MJO mode and the BSISO mode (Fig. 8) are in good agreement with those in previous studies. It is clear that the MJO mode and the BSISO mode have different propagation tendencies, and thus life cycles. A convective anomaly associated with the MJO mode starts to appear over Africa-western Indian Ocean at phase 1. Then it continues to move eastward to the date line (phase 8) all trapped near and along the equator with coupled Kelvin-Rossby wave response nearly symmetric about the equator. Eastward propagation of the convective anomaly in the western hemisphere is not necessarily apparent in this composite, while a circum-global signal in convection may appear in a composite with more emphasis on the ISO behavior in the western hemisphere (Kikuchi and Takayabu 2003).

A convective anomaly associated with the BSISO mode starts to appear in the equatorial central Indian Ocean at phase 1. Then northward propagation of the convection is pronounced in the Indian Ocean with a weak eastward propagation along the equator (phase 2–4), which makes an elongated northwest–southeast band of convection. The southeastern part of the convective anomaly re-intensifies over the South China Sea and the Philippine Sea at phase 5. Northward propagation appears to dominate over the Indian Ocean and the western Pacific with a salient feature of OLR seesaw between the equatorial Indian Ocean and the Philippine Sea. The accompanied circulation is characterized by asymmetric coupled Kelvin-Rossby wave response with stronger amplitude in the northern hemisphere. In addition, a weak eastward propagation of convection can be seen along the ITCZ traveling the North Pacific.

5.2 Annual variation

How the annual variation of the ISO is represented by the bimodal ISO index is discussed. The discussion includes a validity check of the method as well as scientific findings. Specific questions to be considered are the following: (1) *Does the bimodal ISO index choose ISO events fairly throughout the year?* (2) *Does the MJO (BSISO) mode never predominate during boreal summer (winter)?* (3) *When does the predominant ISO mode tend to shift one regime to the other?* Figure 9 shows the average numbers of significant ISO events assigned to the MJO mode and

Fig. 7 Phase space representation of the state of (**a**) the MJO mode (PC$_2$, PC$_1$) and (**b**) the BSISO mode (PC$_1$, PC$_2$) for the period 1979–2009. The state of the ISO categorized as eight phases are used for the following discussion. The approximate positions of the major convective area at some phases are also denoted. Note that each PC is normalized by one standard deviation of the corresponding PCs during the period each EEOF analysis was performed to obtain the EEOFs
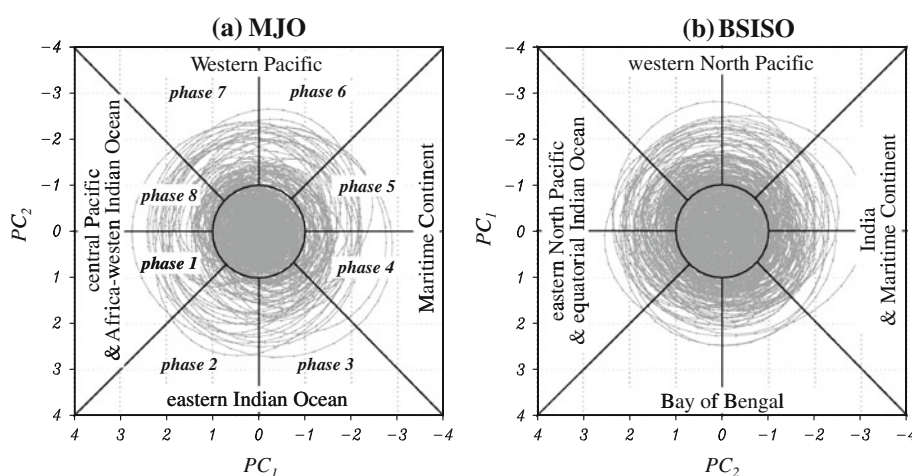
Fig. 8 Composite life cycle of (**a**) the MJO mode and (**b**) the BSISO mode. OLR anomalies (shades and contours of 5 Wm^{-2}) and 850 hPa horizontal winds (*vectors*). Significant values at the 99% level according to the *t* test with degree of freedom being one sixth of the number of composite samples (taking into account of persistence) are only drawn. The number of composite samples are denoted in the *upper right* corner of each *panel*
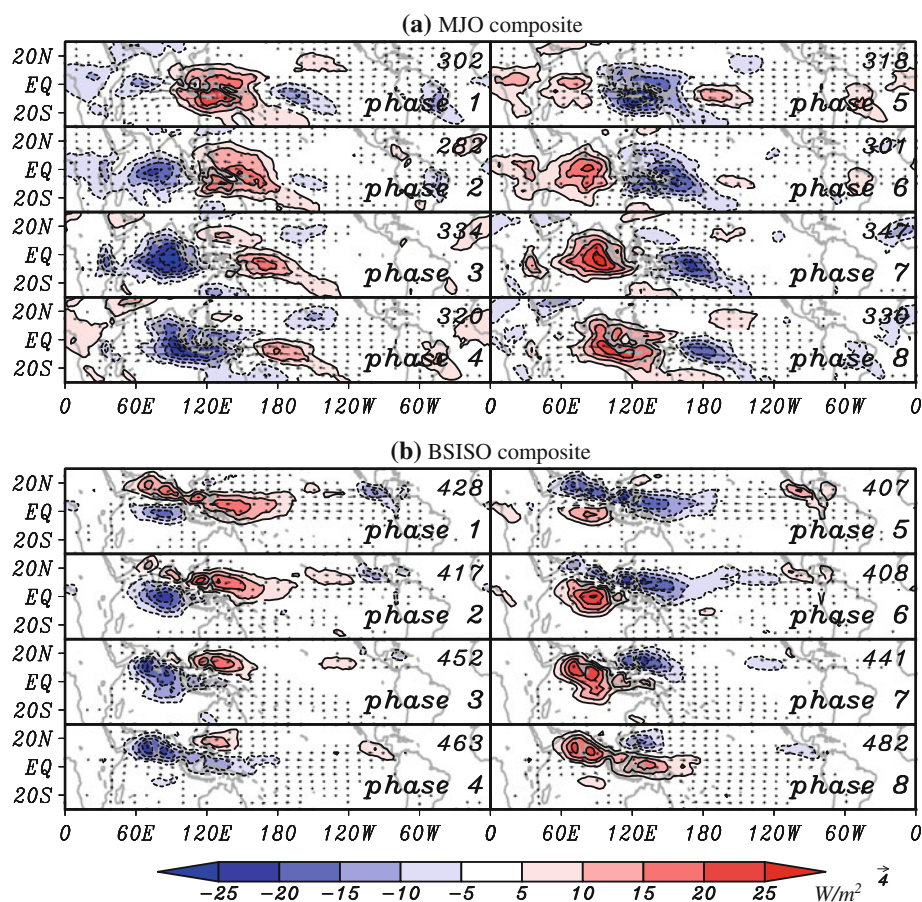

the BSISO mode, which were used to construct the composite (Fig. 8), as a function of calendar month. The total number of significant ISO days (MJO plus BSISO) varies little throughout the year. A clear transition of the annual cycle of the ISO type is found: from December to April almost all ISO events are assigned to the MJO mode, while from June to October almost all ISO events are assigned to the BSISO mode. May and November appear to be

transitional months. Of course, the feature addressed above is consistent with Fig. 4.

6 Real time monitoring

Since the ISO has considerable effect on other phenomena such as tropical cyclogenesis and active-break cycles of
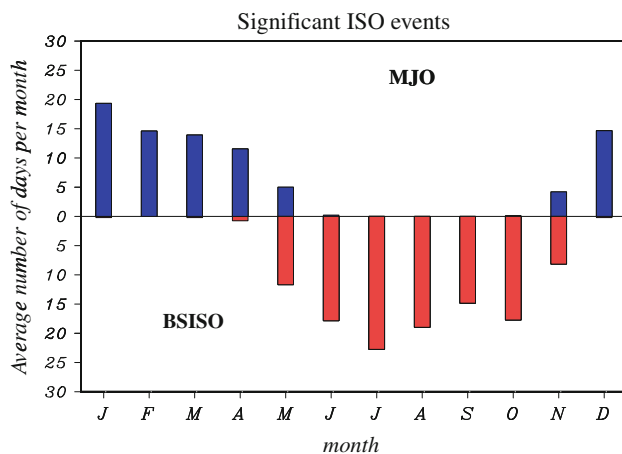
Fig. 9 Average number of days during which significant ISO is present in a month. The days are normalized such that they are the ratio of the number of days classified as the significant MJO mode (*upper*) or significant BSISO mode (*lower*) to the available number of days during 1979–2009 times the number of days in the month of common year

monsoon systems, monitoring the state of the real-time ISO is of great practical importance. In real time monitoring, extraction of variability associated with the ISO is the crucial and challenging process to accomplish; ordinary time filters are impractical because they require future values. Alternatively, in essence, processes are required to remove higher- and lower-frequency variability. In the pioneering work, WH04 used multivariables (OLR and zonal winds at 200 and 850 hPa) meridionally averaged over 15°S–15°N to remove higher-frequency variability; fewer higher-frequency variations have a structure similar to the ISO in the averaged multivariables. In addition, they subtracted the climatological mean and annual cycle to remove the influence of the seasonal cycle, interannual variability linearly correlated with a measure of El Niño in SST to remove the influence of El Niño, and a 120 day mean of the previous 120 days to remove any further aspects of interannual variability and decadal variability and trend.

The bimodal ISO index, on the other hand, was not intended to be developed for real time monitoring, however, we found that it can be easily applied for that purpose. The use of the EEOF analysis with the current setting provides a strong constraint on the spatial-temporal evolution of organized convection which is unique to the ISO and thereby is little shared with other phenomena on shorter and longer timescales such as El Niño. In the end, the OLR anomaly field used for real time monitoring can be obtained by somewhat simpler processes as follows: subtraction of climatological mean and three harmonics of the climatological annual cycle based on the period of record 1979–2009, and a 40 day mean of the previous

40 days to remove lower frequency variability, and applying 5 day tapered running mean to remove higher frequency variability. The number of days of the mean subtraction (40) was determined based on a statistical analysis of the relationship between the intraseasonal time-filtered field and the anomaly field for real time monitoring. Real time PCs of the MJO mode and the BSISO mode can be obtained by projecting the OLR anomaly fields consisting of 3 time steps with −10, −5, and 0 day lags onto each mode derived from the intraseasonal time-filtered historical data (Sect. 4.1). An example of real time monitoring is shown in Fig. 10.[1] It is evident that the real time monitoring time series of both modes primarily capture intraseasonal variations and are well correlated with intraseasonal time-filtered (final) products.

That notion is supported by a statistical analysis of 30 year data during 1979–2009 (Table 3). The correlations between the real time monitoring and the final products are substantially high (~ 0.9), especially in the target season of each mode (e.g., DJF for the MJO mode). Thus the bimodal ISO index provides a reliable objective measure for real time monitoring. A further careful treatment to remove higher- and lower-frequency component based on a sophisticated technique such as the one developed by Arguez et al. (2008) may even improve the performance in real time monitoring.

7 Summary

To accurately reflect the annual variation of the tropical intraseasonal oscillation (ISO), a bimodal ISO index is proposed, which relies on two modes with distinct life cycles of the ISO convection. Each mode was identified with the extended empirical orthogonal function (EEOF) analysis for 31 years (1979–2009) OLR data. The MJO mode represents the typical ISO behavior during boreal winter, when eastward propagation is predominant. The BSISO (boreal summer ISO) mode represents the typical ISO behavior during boreal summer, when northward propagation is prominent over the northern Indian Ocean and western North Pacific. The state of the ISO at any given time of the year, therefore, can be expressed in terms of both the MJO mode and the BSISO mode, which provides essential information for the bimodal ISO index.

Based on that information, we further demonstrate how the dominant ISO mode at any given time can be objectively determined. The bimodal ISO index well correlates with the Wheeler and Hendon's (2004) all season ISO index, and in addition succeeds in highlighting the annual

---

[1] Historical and real time bimodal ISO index is available from the author at URL: http://www.iprc.soest.hawaii.edu/~kazuyosh.

Fig. 10 Real time monitoring of ISO in terms of (*upper*) the MJO mode and (*lower*) the BSISO mode. *Green lines* represent time series of real time PCs at each time and *black lines* represent time series of PCs of a complete bandpass filtered field. Bandpass filtered fields within 70 days of the end point are not available
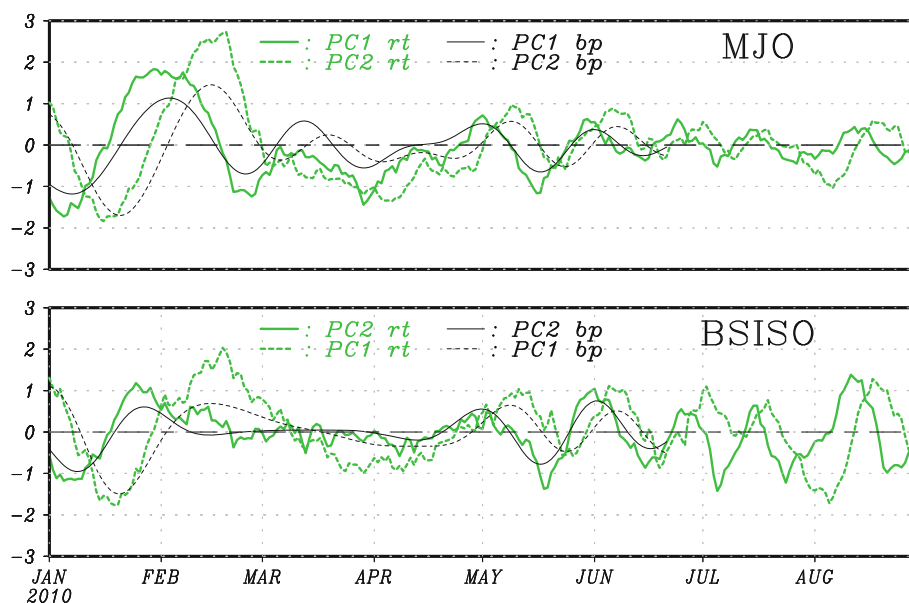
Table 3 Serial correlations of the MJO mode and the BSISO mode between real time monitoring and bandpass filtered time series for 1979–2009

	MJO			BSISO		
	All	DJF	JJA	All	DJF	JJA
PC$_1$	0.89	0.90	0.87	0.91	0.87	0.92
PC$_2$	0.90	0.91	0.86	0.90	0.85	0.92

variation of the ISO characteristics. It is shown that the MJO (BSISO) mode exists almost exclusively from December to April (June–October). May and November are climatological transitional months when the predominant mode changes from one to the other. The ability of the bimodal index to identify the dominant ISO patterns at a given time can be of great importance on understanding interaction processes of the ISO with other phenomena. For instance, a consideration of how and why such seasonal transition of the dominant mode occurs may lead to a better understanding of the interaction between the ISO and the Asian-Australian monsoon systems (e.g., Waliser et al. 2009). It is also suggested that when discussing an interaction process with the ISO in spring and fall, a careful treatment of the ISO is required.

The use of the EEOF analysis, which relies on the spatial-temporal patterns of the ISO, appears to add some advantages. The bimodal ISO index tends to chose well-defined ISO events. Consequently, the composite life cycles of the ISO based on the bimodal ISO index can account for more variances than those based on the WH04 index by at least 50% for the two solstice seasons. Also by the same nature, the bimodal ISO index has reliable performance in real time monitoring.

In conclusion, the bimodal ISO index is useful not only for further studies on historical data analyses but also for practical purposes (e.g., real time monitoring). The careful treatment of the ISO over the course of a year provides the basis for assessing models' reproduction of the ISO and advancing our understanding of predictability of the ISO, because the characteristics of the ISO, which are critical information, undergo the strong seasonal variations.

References

Annamalai H, Sperber KR (2005) Regional heat sources and the active and break phases of boreal summer intraseasonal (30–50 day) variability. J Atmos Sci 62:2726–2748

Arguez A, Yu P, O'Brien JJ (2008) A new method for time series filtering near endpoints. J Atmos Ocean Technol 25:534–546

Bosilovich MG, Schubert SD, Rienecker M, Todling R, Suarez M, Bacmeister J, Gelaro R, Kim G-K, Stajner I, Chen J (2006) NASA's modern era retrospective-analysis for research and applications. US CLIVAR Var 4:5–8

Chen SS, Houze RA Jr (1997) Diurnal variation and life-cycle of deep convective systems over the tropical pacific warm pool. Quart J Roy Met Soc 123:357–388

Duchon CE (1979) Lanczos filtering in one and two dimensions. J Appl Meteorol 18:1016–1022

Hendon HH, Liebmann B (1990) A composite study of onset of the Australian summer monsoon. J Atmos Sci 47:2227–2240

Hendon HH, Salby ML (1994) The life cycle of the Madden-Julian oscillation. J Atmos Sci 51:2225–2237

Higgins RW, Shi W (2001) Intercomparison of the principal modes of interannual and intraseasonal variability of the North American monsoon system. J Clim 14:403–417

Hsu HH (1996) Global view of the intraseasonal oscillation during northern winter. J Clim 9:2386–2406

Ichikawa H, Yasunari T (2008) Intraseasonal variability in diurnal rainfall over New Guinea and the surrounding oceans during austral summer. J Clim 21:2852–2868

Jones C, Carvalho LMV, Higgins RW, Waliser DE, Schemm JKE (2004) Climatology of tropical intraseasonal convective anomalies: 1979–2002. J Clim 17:523–539

Julian PR, Madden R (1981) Comments on a paper by T. Yasunari, a quasi-stationary appearance of 30–40-day period in the cloudiness fluctuations during the summer monsoon over India. J Meteor Soc Jpn 59:435–437

Kajikawa Y, Yasunari T (2005) Interannual variability of the 10–25- and 30–60-day variation over the South China Sea during boreal summer. Geophys Res Lett 32:L04710. doi: 10.1029/2004 GL021836

Kayano MT, Kousky VE (1999) Intraseasonal (30–60 day) variability in the global tropics: principal modes and their evolution. Tellus 51:373–386

Kemball-Cook S, Wang B (2001) Equatorial waves and air-sea interaction in the boreal summer intraseasonal oscillation. J Clim 14:2923–2942

Kessler WS, McPhaden MJ, Weickmann KM (1995) Forcing of intraseasonal Kelvin waves in the equatorial Pacific. J Geophys Res 100:10613–10631

Kikuchi K, Takayabu YN (2003) Equatorial circumnavigation of moisture signal associated with the Madden-Julian oscillation (MJO) during boreal winter. J Meteor Soc Jpn 81:851–869

Kikuchi K, Wang B (2010) Formation of tropical cyclones in the northern Indian Ocean associated with two types of tropical intraseasonal oscillation modes. J Meteor Soc Jpn 88:475–496

Knutson TR, Weickmann KM (1987) 30–60 day atmospheric oscillations: composite life-cycles of convection and circulation anomalies. Mon Wea Rev 115:1407–1436

Lau KM, Chan PH (1985) Aspects of the 40–50 day oscillation during the northern winter as inferred from outgoing long wave radiation. Mon Wea Rev 113:1889–1909

Lau KM, Chan PH (1986) Aspects of the 40–50 day oscillation during the northern summer as inferred from outgoing long wave radiation. Mon Wea Rev 114:1354–1367

Lau KM, Chan PH (1988) Intraseasonal and interannual variations of tropical convection: a possible link between the 40–50 day oscillation and ENSO? J Atmos Sci 45:506–521

Lau KMW, Waliser DE (eds) (2005) Intraseasonal variability in the atmosphere-ocean climate system. Springer, Berlin, p 436

Liebmann B, Smith CA (1996) Description of a complete (interpolated) outgoing longwave radiation dataset. Bull Am Meteor Soc 77:1275–1277

Lorenz DJ, Hartmann DL (2006) The effect of the MJO on the North American monsoon. J Clim 19:333–343

Madden RA (1986) Seasonal-variations of the 40–50 day oscillation in the tropics. J Atmos Sci 43:3138–3158

Madden RA, Julian PR (1971) Detection of a 40–50 day oscillation in the zonal wind in the tropical Pacific. J Atmos Sci 28:702–708

Madden RA, Julian PR (1972) Description of global-scale circulation cells in tropics with a 40–50 day period. J Atmos Sci 29:1109–1123

Madden RA, Julian PR (1994) Observations of the 40–50-day tropical oscillation: a review. Mon Wea Rev 122:814–837

Maloney ED, Hartmann DL (1998) Frictional moisture convergence in a composite life cycle of the Madden-Julian oscillation. J Clim 11:2387–2403

Maloney ED, Hartmann DL (2000a) Modulation of eastern north Pacific hurricanes by the Madden-Julian oscillation. J Clim 13:1451–1460

Maloney ED, Hartmann DL (2000b) Modulation of hurricane activity in the Gulf of Mexico by the Madden-Julian oscillation. Science 287:2002–2004

McBride JL, Davidson NE, Puri K, Tyrell GC (1995) The flow during TOGA COARE as diagnosed by the BMRC tropical analysis and prediction system. Mon Wea Rev 123:717–736

Miller AJ, Zhou S, Yang SK (2003) Relationship of the Arctic and Antarctic oscillations to the outgoing longwave radiation. J Clim 16:1583–1592

Molinari J, Vollaro D (2000) Planetary- and synoptic-scale influences on eastern Pacific tropical cyclogenesis. Mon Wea Rev 128:3296–3307

Moon J-Y, Wang B, Ha K-J (2010) ENSO regulation of MJO teleconnection. Clim Dyn, (in press)

Rui H, Wang B (1990) Development characteristics and dynamic structure of tropical intraseasonal convection anomalies. J Atmos Sci 47:357–379

Salby ML, Hendon HH (1994) Intraseasonal behavior of clouds, temperature, and motion in the tropics. J Atmos Sci 51:2207–2224

Slingo JM, Rowell DP, Sperber KR, Nortley E (1999) On the predictability of the interannual behaviour of the Madden-Julian oscillation and its relationship with El Nino. Quart J Roy Met Soc 125:583–609

Takayabu YN, Iguchi T, Kachi M, Shibata A, Kanzawa H (1999) Abrupt termination of the 1997–1998 El Nino in response to a Madden-Julian oscillation. Nature 402:279–282

von Storch H, Xu J (1990) Principal oscillation pattern analysis of the 30–60-day oscillation in the tropical troposphere. Clim Dyn 4:175–190

Waliser DE, Murtugudde R, Lucas LE (2003a) Indo-Pacific Ocean response to atmospheric intraseasonal variability: 1. Austral summer and the Madden-Julian oscillation. J Geophys Res 108(C5):3160. doi: 10.1029/2002JC001620

Waliser DE, Lau KM, Stern W, Jones C (2003b) Potential predictability of the Madden-Julian oscillation. Bull Am Meteor Soc 84:33–50

Waliser DE, Murtugudde R, Lucas LE (2004) Indo-Pacific Ocean response to atmospheric intraseasonal variability: 2. Boreal summer and the intraseasonal oscillation. J Geophys Res 109:C03030. doi: 10.1029/2003JC002002

Waliser D, Sperber K, Hendon H, Kim D, Wheeler M, Weickmann K, Zhang C, Donner L, Gottschalck J, Higgins W, Kang IS, Legler D, Moncrieff M, Vitart F, Wang B, Wang W, Woolnough S, Maloney E, Schubert S, Stern W (2009) MJO simulation diagnostics. J Clim 22:3006–3030

Wang B, Rui H (1990) Synoptic climatology of transient tropical intraseasonal convection anomalies: 1975–1985. Meteor Atmos Phys 44:43–61

Wang B, Webster P, Kikuchi K, Yasunari T, Qi YJ (2006) Boreal summer quasi-monthly oscillation in the global tropics. Clim Dyn 27:661–675

Weare BC, Nasstrom JS (1982) Examples of extended empirical orthogonal function analyses. Mon Wea Rev 110:481–485

Webster PJ, Magana VO, Palmer TN, Shukla J, Tomas RA, Yanai M, Yasunari T (1998) Monsoons: processes, predictability, and the prospects for prediction. J Geophys Res 103:14451–14510

Wheeler MC, Hendon HH (2004) An all-season real-time multivariate MJO index: development of an index for monitoring and prediction. Mon Wea Rev 132:1917–1932

Yasunari T (1979) Cloudiness fluctuations associated with the northern hemisphere summer monsoon. J Meteor Soc Jpn 57:227–242

Zhang CD (2005) Madden-Julian oscillation. Rev Geophys 43:RG2003. doi:10.1029/2004RG000158

Zhang CD, Dong M (2004) Seasonality in the Madden-Julian oscillation. J Clim 17:3169–3180

Zhang CD, Hendon HH (1997) Propagating and standing components of the intraseasonal oscillation in tropical convection. J Atmos Sci 54:741–752